Supernumerary Robotic Limbs for Human Body Support

Federico Parietti, *Student Member, IEEE*, and Harry Asada, *Member, IEEE*

***Abstract*—A robot attached to a human body can support the human when performing tasks in dangerous environments or when taking postures that are fatiguing and uncomfortable. This paper presents a new type of supernumerary robotic limbs (SRL) that supports the human body against floors, walls, and surrounding structures so that the human can perform a task safely, comfortably, and stably. First, the use of wearable robots for securing and supporting a human body is discussed, followed by an SRL design concept. The SRL is worn around the waist and can brace the human body by making contact with a wall, grasping a rail, or being anchored to the floor. Quasi-static stability and compliance with which the body is supported are analyzed. Two control methods for stabilizing the body support system are considered: one is null-space stabilization using Hessian matrices, and the other is joint servo stiffness, based on the Jacobian. A prototype robot is designed and tested. Potential applications of the SRL in diverse fields are discussed.**

***Index Terms*—Human support, stiffness control, wearable extra limbs.**

I. Introduction

HUMAN workers play an essential role in the construction of complex structures such as airplanes, ships, and high-rise buildings. In all of these fields, automation has not been widely adopted for several reasons. First, trained personnel can quickly learn and execute difficult tasks, responding to unforeseen problems thanks to previous experiences and common sense. Autonomous robots do not yet possess such flexibility or the capacity to deal with a complex and unpredictable environment. Moreover, traditional industrial robots are not safe for operation in proximity to workers, and their limited mobility does not allow them to navigate structures designed for humans (e.g., scaffolds and stairs) or to reliably operate dangerous hand tools (e.g., power drills and jackhammers).

Even though their contribution to high added-value manufacturing is irreplaceable, human workers would greatly benefit from robots that are able to support and help them in the most fatiguing or dangerous tasks. Falls are the leading cause for injuries on construction sites and one of the major sources of risk in manufacturing facilities [1]. Regulations require the installation of fall prevention systems [2], but these are usually passive and cannot follow workers everywhere or prevent slips. Overexertion is another common cause of injury for manufacturing and construction employees [3]. Fatigue also results in decreased productivity [3]. Additionally, the manufacturing workforce is characterized by a marked aging trend [4]. For all of these reasons, it would be highly advantageous if workers could make use of a wearable robot that is able to support them in the most demanding tasks, while also securing them to the environment in order to avoid falls.

In robotic research, exoskeletons have been one of the most popular approaches to wearable human augmentation systems [5]. Leg exoskeletons have found many rehabilitation and military applications [6], [7], while their use in industrial settings is still in its early phase [8]. Arm exoskeletons have been mainly used for rehabilitation research [9]. From the point of view of actuation, exoskeletons can be classified as active or passive. The former can provide the high torques required to follow and support human motion but have weight and battery duration issues [10]. The latter are lightweight and compact but useful only in a limited range of scenarios, such as partial weight compensation [11]. If we consider their structure, exoskeletons can be divided into two groups: rigid and soft systems. Rigid exoskeletons replicate the jointed structure of human bones, reducing the loads on the wearer [12]. The drawbacks are their weight and the fact that they tend to constrain human motion [11]. Soft systems, on the other hand, do not get in the way of the user and are lightweight but apply additional loads to human joints [13].

Workers often make use of passive support tools, such as stools and ladders. These tools can compensate for the weight of the user, but must be manually moved where needed. Moreover, they cannot assist the stability of the workers and do not protect them from falls and slips. Passive safety systems such as body harnesses, on the other hand, protect workers from falls but cannot increase their stability or reduce their workload and have a limited range.

Active and passive industrial lifting support systems can be comfortably worn by workers and reduce exertion forces on their lower back [14], [15]. However, they cannot stabilize the posture of the user or prevent falls. When active, these systems have advantages or shortcomings similar to leg exoskeletons.

In this paper, we introduce a novel kind of wearable robot designed to provide support and enhanced safety to manufacturing workers (see Fig. 1). The system, named supernumerary robotic limbs (SRL), consists of additional robotic arms worn through a backpack-like harness. The artificial limbs coordinate with the users and help them perform complicated or fatiguing tasks. Being kinematically independent from the human,

Manuscript received August 18, 2015; revised December 15, 2015; accepted December 29, 2015. This paper was recommended for publication by Associate Editor E. Yoshida and Editor I.-M. Chen upon evaluation of the reviewers' comments.

The authors are with the Department of Mechanical Engineering, Massachusetts Institute of Technology, Cambridge, MA 02139 USA (e-mail: yfwu@mit.edu; asada@mit.edu).

This paper has supplementary downloadable material available at http://ieeexplore.ieee.org.

Color versions of one or more of the figures in this paper are available online at http://ieeexplore.ieee.org.

Digital Object Identifier 10.1109/TRO.2016.2520486

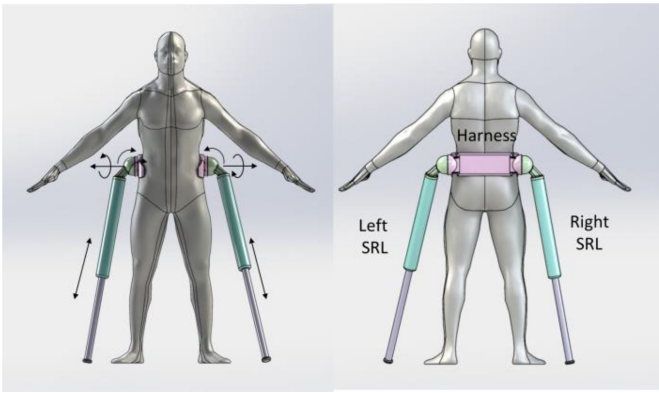

Fig. 1. Design concept of SRL: Two extra robotic limbs are worn around the waist. Each robotic limb has three DOFs: two rotational joints and one prismatic joint.

the SRL can provide support without constraining user motion. The workspace of the robotic arms allows them to behave as additional legs, arms, or even reach areas that are outside of the human workspace. The SRL has been designed to help workers in a wide range of manufacturing tasks, from manipulation to load lifting [16], [17]. In the following sections, we will explore the use of the SRL to compensate for the weight of workers and to stabilize them while operating in uncomfortable positions.

An early version of the paper has been published in conference proceedings. In [18], a different type of prototype design was presented and was compared with exoskeletons in terms of load-bearing efficiency. Optimal configuration of the robotic limbs was obtained for minimizing the human effort in bearing a load. This paper presents a new design concept of SRL for supporting a human body and detailed analysis and synthesis of body support stability will be presented by examining the stiffness matrix with which the body is supported. The theoretical results will be implemented on a new prototype SRL.

II. Design Concept

A. Mechanism

The system consists of a pair of robotic limbs, a harness, and a control unit. Each robotic limb has three degrees of freedom (DOFs), allowing the endpoint to reach an arbitrary position in space. The harness secures the robotic limbs to the hip bone of the user. As the primary objective of this robot is to provide support, it is reasonable to place the robot at the waist, which is simultaneously near the body's center of mass and will not interfere with upper body motion. Multiple straps are used for securing the harness that extends to the thighs and shoulders. One of the major functional requirements for the SRL is to bear a large load for a long time while using minimal energy. A prismatic joint with a high gear ratio is not back-drivable; hence, it can bear a load without consuming energy. The SRL in Fig. 1 exploits this feature. Once the prismatic joint is fixed at a certain length, it serves as a "stick." Consequently, most of the load is borne in the longitudinal direction of each stick, the orientation of which is varied with two revolute joints placed on the base of the robot closer to the harness.

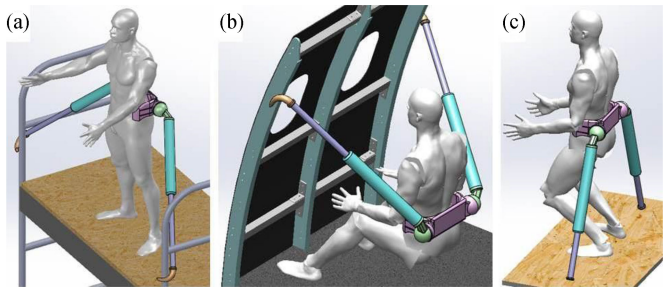

Fig. 2. Potential uses of the SRL. (a) Bracing against a scaffold for safety. (b) Suspension from a wall/ceiling. (c) Support from the floor.

B. Potential Uses

The SRL can be applied to various tasks to facilitate a human in performing dangerous, laborious, or difficult jobs. Fig. 2 shows a collection of potential uses of SRL. In Fig. 2(a), the human wearing the SRLs is braced against a rail or a scaffold beam for safety. Here, each SRL is equipped with a gripper at the end of the stick to secure the endpoint to the rail. This type of body bracing for safety is useful for various field works, including construction, utility infrastructure maintenance, and disaster response works as well as an astronaut's Extra-Vehicular Activities (EVA). In Fig. 2(b), the human has to reach a low position to work on the floor or near the floor for a long period of time. The SRLs suspend the human body so that the human does not have to crouch or take an uncomfortable posture. In Fig. 2(c), the human is taking a half-crouch posture, which is laborious if the posture must be kept for a long time. The SRLs support the body from the floor to reduce the load on the knees and ankles. These body suspension applications can be found in various factory works, including aircraft fuselage assembly and automobile assembly, as well as in construction and field works.

C. Design and Control Issues

When performing a task, workers often need to change their posture and position. Examples include picking up a tool from a nearby toolbox, working at a location slightly away from the current position, and checking the side of an object. In all of these situations, workers need to move sideways, turn, or bend down freely in the vicinity of their current position. To be a useful aid for workers, the SRL must support their weight without restraining their motion. The six active joints of the SRL can provide users with a flexible body support that aids them in the execution of a manufacturing task. The joints of the SRL can be controlled in diverse modes: pure position-control mode, compliance-control mode, torque control mode, and nonback-drivable mode. Combining these modes and assigning them to the individual joints will allow the SRL to provide the human with various types of support that can 1) reduce the human gravity load, 2) transport the body in a desired direction, 3) stabilize the body, and 4) allow the body to move freely without constraints in selected directions.

In Fig. 2(b) and (c), the user is either suspended from above or supported from the floor in order to reduce the weight-bearing effort. At a desired location, the prismatic joints of both SRLs may be left idle to save energy. If the gear ratio is large enough

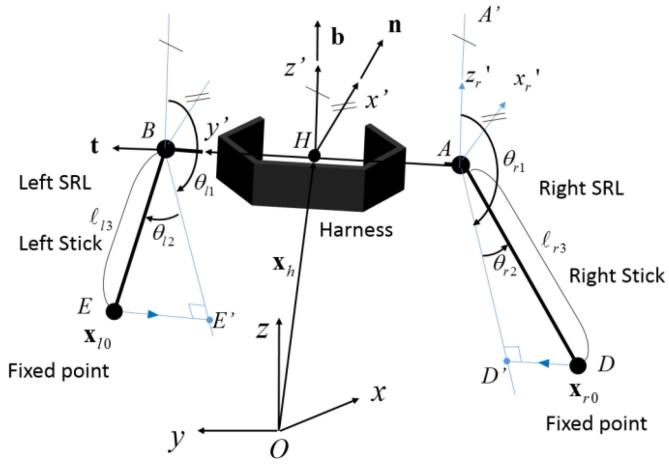

Fig. 3. Schematic of the SRL system, coordinate frames, and joint angles. Point *D*' is the projection of point *D*, the fixed point of the right SRL, onto the $A - x_r{}'z_r{}'$ plane; the revolute joint angles are defined as $\theta_{r1} = \angle A'AD'$, $\theta_{r2} = \angle D'AD$; the left revolute angles are defined in a similar manner.

to support the gravity load with friction, no energy is required for supporting the human body. The nonbackdrivable mode can save energy when supporting a gravity load. A high gear ratio in the prismatic joints would also make it easier for the SRL to lift and transport the user with position control. In Fig. 2(b), for example, the human body can be moved sideways; elongating the left robotic limb and contracting the right can move the user to the right and vice versa. See the supplemental video. Once the worker reaches the designed height and lateral position, the prismatic joints are switched off, and the SRL stops in that position (nonbackdrivable mode).

While the two robotic limbs can support the human body, the specific SRL configuration may be at an unstable static equilibrium. In Fig. 2(c), for example, the support offered by the SRL may collapse as the user rotates about the vertical axis. This instability may be eliminated or alleviated with high stiffness control of the revolute joints. More generally, the compliance with which the human body is supported may be varied by coordinating the servoed joints based on compliance control. The two revolute joints in each robotic limb are suitable for compliance control. Coordination of the four revolute joints will allow us to synthesize a desired compliance in the task space so that the human body may be supported with a desired compliance in selected directions. In particular, the body should be supported stably and safely but should not be overconstrained.

The stability of body support and the suspension compliance depend on the configuration of the SRL, i.e., where the end effectors are secured to the surrounding environment. Among multiple locations for possible bracing, the SRL should select a desired configuration that allows it to support the human body most effectively and efficiently. Unlike lower exoskeletons, where servoed joints are attached to the human joints, the SRL is not kinematically constrained to the human limbs. The robotic limbs can take an arbitrary configuration, independent of the human limbs. This opens up the possibility of optimizing body support performance with respect to 1) support stability, 2) reduction of human effort, and 3) reduction of energy consumption. In the following sections, we will focus on stability in supporting the human body, presenting detailed analysis and synthesis of a stiffness matrix, including null-space stabilization and joint servo stiffness control.

III. Support Stability

A. Basic Formulation

Fig. 3 shows a schematic of the SRL system with the right SRL attached to the right side of the harness (Point *A*) and the left SRL to the other side (Point *B*). The position of the center point of the harness is denoted x_h, y_h, z_h with reference to the base coordinate system, $O - xyz$. Another coordinate frame, *H - x'y'z'*, is attached to the harness and its orientation is represented by three angular displacements: roll ϕ_x, pitch ϕ_y, and yaw ϕ_z relative to the base coordinate system. Let $\mathbf{n}, \mathbf{t}$, and $\mathbf{b}$ be the unit vectors pointing in the directions of the harness coordinate axes *x*', *y*', and *z*', respectively. Concatenating these unit vectors in a 3×3 matrix, we can write the compact expression

$$[\mathbf{n}, \mathbf{t}, \mathbf{b}] = \mathbf{R}_z(\phi_z)\mathbf{R}_y(\phi_y)\mathbf{R}_x(\phi_x) \tag{1}$$

where $\mathbf{R}_x(\phi_x)$, $\mathbf{R}_y(\phi_y)$, and $\mathbf{R}_z(\phi_z)$ are 3×3 rotation matrices about the *x*-, *y*-, and *z*-axes, respectively.

Each SRL has two revolute joints and one prismatic joint with joint displacements denoted as θ_1, θ_2, and ℓ_3, respectively. The three joint variables form a "polar coordinate system" relative to the harness coordinate frame *H - x'y'z'*, as shown in Fig. 3. Each SRL has a gripper or a clamp at the tip of the stick for securing its endpoint to the surrounding environment. For a given harness position and orientation and a given location of the endpoint fixed to the environment, the joint angles of each SRL can be obtained analytically. Solving a simple inverse kinematic problem, we can write them as a vectorial function

$$\begin{pmatrix} \theta_1 \\ \theta_2 \\ \ell_3 \end{pmatrix} = \mathbf{g}(x_h, y_h, z_h, \phi_x, \phi_y, \phi_z; x_0, y_0, z_0) \tag{2}$$

where x_0, y_0, and z_0 are coordinates of the fixed point. Similar equations can be obtained for both SRLs. Denoting the right SRL with a subscript *r* and the left SRL by *l*, we can collectively write the joint displacements as a vectorial function of the harness position and orientation for given fixed points of both SRLs

$$\mathbf{q} = \begin{pmatrix} \theta_{r1} \\ \theta_{r2} \\ \ell_{r3} \\ \theta_{l1} \\ \theta_{l2} \\ \ell_{l3} \end{pmatrix} = \begin{pmatrix} \mathbf{g}_r(x_h, y_h, z_h, \phi_x, \phi_y, \phi_z; x_{r0}, y_{r0}, z_{r0}) \\ \mathbf{g}_l(x_h, y_h, z_h, \phi_x, \phi_y, \phi_z; x_{l0}, y_{l0}, z_{l0}) \end{pmatrix}. \tag{3}$$

Assuming that the movable range of each joint is properly limited to avoid multiple solutions to the inverse kinematic problem, the six variables of the harness position and orientation $x_h, y_h, z_h, \phi_x, \phi_y, \phi_z$ completely determine the joint displacements of both SRL limbs for given right and left fixed points,x_{r0}, y_{r0}, z_{r0} and x_{l0}, y_{l0}, z_{l0}. In other words, the six

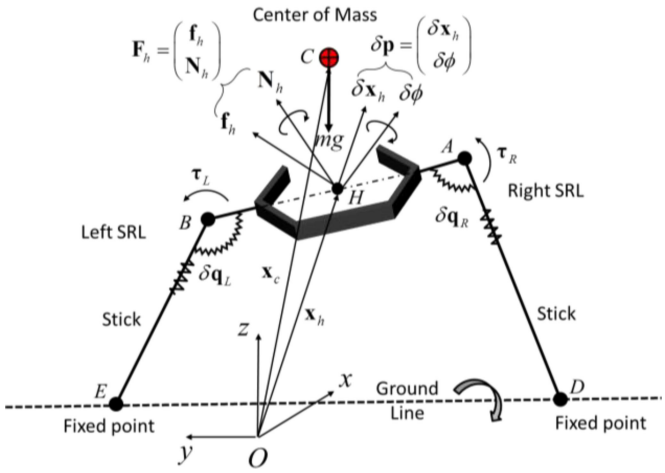

Fig. 4. Forces and moments acting on the SRL system.

variables $x_h, y_h, z_h, \phi_x, \phi_y, \phi_z$ provide a complete and independent set of generalized coordinates that locate the system.

Differentiating the above kinematic equation yields the Jacobian matrix relating infinitesimal joint displacements to infinitesimal harness position and orientation

$$d\mathbf{q} = \mathbf{J} d\mathbf{p}, \quad \mathbf{J} = \begin{pmatrix} \frac{d\mathbf{g}_r}{d\mathbf{p}} \\ \frac{d\mathbf{g}_l}{d\mathbf{p}} \end{pmatrix} \in \Re^{6\times 6} \tag{4}$$

where $d\mathbf{p} = (dx_h, dy_h, dz_h, d\phi_x, d\phi_y, d\phi_z)^T$.

Fig. 4 shows all the forces and moments acting on the SRL system that produce work. We assume that the sticks of the SRLs are massless and that the total mass of the human body and the harness is *m* with its center of mass at $\mathbf{x}_c = (x_c\ y_c\ z_c)^T$. The human generates force $\mathbf{f}_h$ and moment $\mathbf{N}_h$ acting on the harness, which are collectively represented as a 6-D vector or wrench: $\mathbf{F}_h = (\mathbf{f}_h^T, \mathbf{N}_h^T)^T$. The two revolute and one prismatic joints of each SRL produce torques τ_1, τ_2 and force f_3, respectively. These joint torques and forces are collectively represented as a 6-D vector $\boldsymbol{\tau} = (\tau_{r1}\ \tau_{r2}\ f_{r3}\ \tau_{l1}\ \tau_{l2}\ f_{l3})^T$. The virtual work done by these forces and moments on the SRL system with both sticks fixed to the environment is given by

$$\delta\text{Work} = mg\delta z_c + \mathbf{F}_h^T \delta\mathbf{p} + \boldsymbol{\tau}^T \delta\mathbf{q}. \tag{5}$$

Since the harness position and orientation $\mathbf{p}$ are generalized coordinates, it can be written as

$$\delta\text{Work} = (mg\mathbf{e}_z^T + \mathbf{F}_h^T + \boldsymbol{\tau}^T \mathbf{J})\delta\mathbf{p} \tag{6}$$

where $\delta z_c = \mathbf{e}_z^T \delta\mathbf{p}$ with $\mathbf{e}_z^T = dz_c/d\mathbf{p} \in \Re^{1\times 6}$. The system is statically balanced if, and only if, the above virtual work vanishes for all $\delta\mathbf{p}$. That is

$$mg\mathbf{e}_z + \mathbf{F}_h + \mathbf{J}^T \boldsymbol{\tau} = 0. \tag{7}$$

The above equilibrium condition provides us with a basic formula for analyzing the effectiveness of body bracing, human efforts, and support stability.

B. Stability Analysis

The SRLs are required to stably support the human body. In this section, we will obtain the stiffness with which the body is supported, followed by its synthesis for stabilization. In analyzing the body support stiffness, we assume that the human does not generate any force other than the gravity force of the body, $\mathbf{F}_h = 0$. The objective of bracing is to reduce the human effort. We consider the situation wherein the human is relaxed at an equilibrium point.

Let $\bar{\mathbf{p}}$ be an equilibrium harness position and orientation, and $\bar{\mathbf{q}}$ be the corresponding joint displacement vector. Consider small displacements from equilibrium coordinates

$$\Delta\mathbf{p} = \mathbf{p} - \bar{\mathbf{p}}, \quad \Delta\mathbf{q} = \mathbf{q} - \bar{\mathbf{q}}. \tag{8}$$

Note that, at equilibrium$\bar{\mathbf{p}}, \bar{\mathbf{q}}$, the static balance conditions are satisfied with joint torques $\bar{\boldsymbol{\tau}}$ as

$$mg\mathbf{e}_z + \mathbf{J}^T \bar{\boldsymbol{\tau}} = 0. \tag{9}$$

Our objective is to obtain reference inputs and feedback control law of the SRLs for stably supporting the body. To this end, we consider that the joint torques are controlled according to the following vector Hookean law:

$$\boldsymbol{\tau} = \bar{\boldsymbol{\tau}} - \mathbf{K}_q \Delta\mathbf{q} \tag{10}$$

where $\mathbf{K}_q \in \Re^{6\times 6}$ is a real symmetric stiffness matrix in the joint space that can be tuned with joint feedback gains. Positive feedback gains produce restoring joint torques toward the equilibrium $\bar{\mathbf{q}}$.

Consider a potential function in the vicinity of the equilibrium point

$$U = mgz_c - \bar{\boldsymbol{\tau}}^T \Delta\mathbf{q} + \frac{1}{2}\Delta\mathbf{q}^T \mathbf{K}_q \Delta\mathbf{q}. \tag{11}$$

The quasi-static stability can be examined with the second derivative of the potential function

$$\frac{d}{d\mathbf{p}}\left(\frac{dU}{d\mathbf{p}}\right)^T = \frac{d}{d\mathbf{p}}(mg\mathbf{e}_z + \mathbf{J}^T \mathbf{K}_q \Delta\mathbf{q} - \mathbf{J}^T \bar{\boldsymbol{\tau}}). \tag{12}$$

To execute the second derivative, we need Hessians given by

$$\mathbf{E}_z \triangleq \frac{d\mathbf{e}_z}{d\mathbf{p}} = \left\{\frac{\partial^2 z_c}{\partial p_j \partial p_k}\right\} \in \Re^{6\times 6} \tag{13}$$

$$\mathbf{H}_i \triangleq \left\{\frac{\partial^2 q_i}{\partial p_j \partial p_k}\right\} \in \Re^{6\times 6}, \quad i = 1, \ldots, 6. \tag{14}$$

Using these Hessians and evaluating the second derivative of the potential function at the equilibrium where $\boldsymbol{\tau} = \bar{\boldsymbol{\tau}}$, we can find the stiffness matrix with which the body is held in equilibrium as

$$\begin{aligned} \mathbf{K}_p(\bar{\mathbf{p}}) &\triangleq \frac{d}{d\mathbf{p}}\left(\frac{dU}{d\mathbf{p}}\right)^T\Bigg|_{\bar{\mathbf{p}}} \\ &= \left(mg\frac{d\mathbf{e}_z}{d\mathbf{p}} + \mathbf{J}^T \mathbf{K}_q \mathbf{J} - \frac{d}{d\mathbf{p}}(\mathbf{J}^T \boldsymbol{\tau})\right)\Bigg|_{\bar{\mathbf{p}}} \\ &= mg\bar{\mathbf{E}}_z + \bar{\mathbf{J}}^T \mathbf{K}_q \bar{\mathbf{J}} - \sum_{i=1}^{6} \bar{\tau}_i \bar{\mathbf{H}}_i \end{aligned} \tag{15}$$

where $\bar{\mathbf{E}}_z = \mathbf{E}_z|_{\bar{\mathbf{p}}}, \bar{\mathbf{J}} = \mathbf{J}|_{\bar{\mathbf{p}}}$, and $\bar{\mathbf{H}} = \mathbf{H}|_{\bar{\mathbf{p}}}$. Note that the above stiffness matrix is represented in the $\mathbf{p}$ space, the coordinates of the harness position and orientation. If this stiffness matrix is positive definite, the equilibrium is stable in the quasi-static sense.

C. Stabilization

Based on the stiffness matrix given by (15), this section addresses how to make the SRL system quasi-statically stable. We consider two ways of making the stiffness matrix positive semi-definite. One is to exploit the Hessian term, the third term in (15), and the other is by the joint servo stiffness, the second term in (15). Combining these two methods of stabilizing the stiffness matrix will lead to an effective means of supporting the human stably.

1) Null-Space Stabilization: The Jacobian matrix is not of full rank, i.e., $\det \mathbf{J} = 0$. This implies that there exists at least one direction in the $\mathbf{p}$ space (one screw) in which displacement $\Delta\mathbf{p}$ does not produce any joint displacement in $\mathbf{q}$. In fact, a rotation of the whole SRL system about the axis connecting both fixed points *D* and *E* does not cause any displacement in the joint space. See the rotation about the broken line *DE*, called the Ground Line in Fig. 4. Consequently, the joint compliance control cannot influence the stiffness in this particular direction, which belongs to the Jacobian null space

$$\Delta\mathbf{p}_{\rm null} \in N(\mathbf{J}). \tag{16}$$

This further implies that both the second and third terms of the body support stiffness $\mathbf{K}_p$ in (15) are not of full rank

$$\det\left(\bar{\mathbf{J}}^T\mathbf{K}_q\bar{\mathbf{J}} - \sum_{i=1}^{6}\bar{\tau}_i\bar{\mathbf{H}}_i\right) = 0. \tag{17}$$

The best we can do is to make the stiffness matrix positive-definite in the range space, which excludes the rotation about Ground Line *DE*.

Remark: The existence of null space also implies that there exists at least one direction of joint torque vector that does not generate any force/moment (wrench) in the $\mathbf{p}$ space. Such a joint torque vector is in the null space of the Jacobian transpose [19]

$$\boldsymbol{\tau}_{\rm null} \in N(\mathbf{J}^T) = [R(\mathbf{J})]^{\perp} \tag{18}$$

where $R(\mathbf{J})$ is the range space of the Jacobian, and $[-]^{\perp}$ represents its orthogonal complement. This joint torque vector indicates an internal force/torque that does not influence the static balance conditions. However, they do influence the body support stiffness through the third term in (15): $-\sum\bar{\tau}_i\bar{\mathbf{H}}_i$.

Since the rank of $\mathbf{J}$ is 5 at most configurations, the dimension of $N(\mathbf{J}^T)$ is 1. Let us write the null joint torque vector as

$$\begin{aligned}\boldsymbol{\tau}_{\rm null} &= \alpha\mathbf{t}_{\rm null}\\ |\mathbf{t}_{\rm null}| &= 1, \quad \mathbf{t}_{\rm null} = \begin{pmatrix} t_1 & t_2 & t_3 & t_4 & t_5 & t_6\end{pmatrix}\end{aligned} \tag{19}$$

where α is a scalar. Substituting this into the Hessian term yields

$$\alpha\mathbf{H}_{\rm null} \triangleq \alpha\sum_{i=1}^{6} t_i\bar{\mathbf{H}}_i. \tag{20}$$

Note that both t_i and $\mathbf{H}_i$ are kinematic quantities, uniquely determined at each $\mathbf{p}$, the harness position and orientation. The 6×6 matrix $\alpha\mathbf{H}_{\rm null}$ provides the "tunable" subspace in which the support stiffness can be varied by tuning the joint torques in the null space. The matrix $\mathbf{H}_{\rm null}$ may contribute to increasing or decreasing the stability in the tunable subspace. Since parameter α may take both positive and negative values, one can always use this Hessian term to improve the stability by selecting the sign of parameter α.

2) Joint Servo Stiffness: The null-space stabilization with $\alpha\mathbf{H}_{\rm null}$ may not be able to stabilize all directions. The joint servo stiffness given by the second term in (15) can be used for making the system quasi-stable in the whole range space. Let $\mathbf{K}_{p-\rm des}$ be a desired or target stiffness in the $\mathbf{p}$ coordinate system, which is positive definite in the range space. Assuming that the null-space stabilization is in place, we can write the conditions for the joint servo stiffness to satisfy as

$$\bar{\mathbf{J}}^T\mathbf{K}_q\bar{\mathbf{J}} = \mathbf{K}_{p-\rm des} - mg\bar{\mathbf{E}}_z + \alpha\mathbf{H}_{\rm null}. \tag{21}$$

Compared with the null-space stabilization, the joint servo stiffness is more complex, requiring active control of joint torques. It is wise to minimize the gains of the joint servo loops, which can be obtained by using the pseudoinverse of the Jacobian

$$\mathbf{K}_q = (\bar{\mathbf{J}}^T)^{\#}[\mathbf{K}_{p-\rm des} - mg\bar{\mathbf{E}}_z + \alpha\mathbf{H}_{\rm null}]\bar{\mathbf{J}}^{\#}. \tag{22}$$

Note that this solution minimizes the norm of the joint feedback gain matrix: $|\mathbf{K}_q|$.

Applying both null-space stabilization and joint servo virtual stiffness, the control law for the robot becomes

$$\boldsymbol{\tau} = \bar{\boldsymbol{\tau}} + \boldsymbol{\tau}_{\mathbf{null}} - \mathbf{K}_{\mathbf{q}}\boldsymbol{\Delta}\mathbf{q}$$

where the total joint torques are given by the sum of the torques needed for static equilibrium [$\bar{\boldsymbol{\tau}}$, (9)], the null-space stabilizing torques [$\boldsymbol{\tau}_{\mathbf{null}}$, (19)], and the P control torques [see (22)].

D. Special Case

Before implementing the above stabilization algorithms on a prototype SRL system, we discuss a special case that is of practical importance. One of the critical requirements for body support SRLs is to minimize the human's effort in keeping a body posture. An ideal case is that the SRL completely supports the human weight so that the human exerts no force and no moment, as assumed in the above analysis: $\mathbf{F}_h = \mathbf{0}$. This can be achieved at a particular configuration of the SRL, which turns out to be useful in most cases. This section will discuss this particular solution.

Consider the case in which both SRL sticks have the same length, $\ell_{r3} = \ell_{l3}$, and the center of mass *C* is directly above the center of the harness at a distance *h* in the direction of unit vector $\mathbf{b}$ so that $\mathbf{x}_c = \mathbf{x}_h + h\mathbf{b}$. When the point C is below the harness, the variable *h* takes a negative value. Furthermore, let us first assume that all the revolute joints of the SRLs generate no torques, $\tau_{r1} = 0,\ \tau_{r2} = 0,\ \tau_{l1} = 0,\ \tau_{l2} = 0$, and the prismatic joints alone bear the gravity load. Under these assumptions, the only possible equilibrium exists when the center lines of

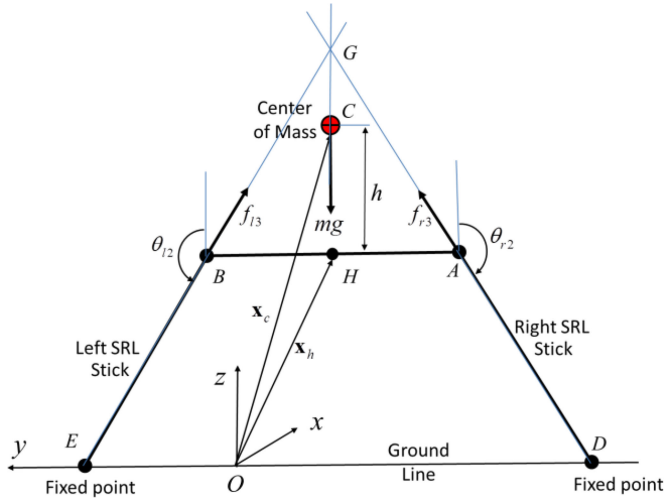

Fig. 5. Symmetric equilibrium configuration.

the right and left SRL sticks and the gravity force vector meet at a single point *G*, as shown in Fig. 5. At this equilibrium, the SRL configuration is symmetric, and the points *A, B, C*, and *H* as well as the fixed points of both SRLs are within the same vertical plane. Consequently, $\theta_{r1} = \theta_{l1} = 0$, $\theta_{r2} = \theta_{r2} = \theta_2$ and $\phi_x = \phi_y = \phi_z = 0,\ y_c = 0$. The prismatic joint forces can be found as

$$\bar{f}_{r3} = \bar{f}_{l3} = -\frac{mg}{2\cos\theta_{r2}}. \tag{23}$$

The Hessian of z_c is given by

$$\bar{\mathbf{E}}_z = \left\{\frac{\partial^2 z_c}{\partial p_j \partial p_k}\right\}\Big|_{\bar{\mathbf{p}}} = \mathrm{diag}(0,\ 0,\ 0,\ -h,\ -h,\ 0). \tag{24}$$

Furthermore, denoting the stiffness of both prismatic joints by k_0, we can write the joint stiffness matrix as

$$\mathbf{K}_q = \mathrm{diag}\,(0,\ 0,\ k_0,\ 0,\ 0,\ k_0) \tag{25}$$

since no revolute joint torques are generated. Substituting (23)–(25) into (15) yields

$$\begin{aligned}\mathbf{K}_p = \ & mg\bar{\mathbf{E}}_z + k_0(\bar{\mathbf{J}}_3^T\bar{\mathbf{J}}_3 + \bar{\mathbf{J}}_6^T\bar{\mathbf{J}}_6) \\ & + \frac{mg}{2}\left(\frac{1}{\cos\theta_{r2}}\bar{\mathbf{H}}_3 + \frac{1}{\cos\theta_{l2}}\bar{\mathbf{H}}_6\right)\end{aligned} \tag{26}$$

where $\mathbf{J}_3$ and $\mathbf{J}_6$ are the third and the sixth rows of the Jacobian matrix

$$\mathbf{J}_3 = \frac{d\ell_{r3}}{d\mathbf{p}} \in \Re^{1\times 6}, \quad \mathbf{J}_6 = \frac{d\ell_{l3}}{d\mathbf{p}} \in \Re^{1\times 6} \tag{27}$$

and the Hessians are given by

$$\mathbf{H}_3 = \frac{d}{d\mathbf{p}}\left(\frac{d\ell_{r3}}{d\mathbf{p}}\right)^T \in \Re^{6\times 6},\ \mathbf{H}_6 = \frac{d}{d\mathbf{p}}\left(\frac{d\ell_{l3}}{d\mathbf{p}}\right)^T \in \Re^{6\times 6}. \tag{28}$$

For $0 \le \theta_2 < \pi/2$, the harness is suspended from a ceiling or a higher place. Therefore, the system is stable. In contrast, for $\pi/2 < \theta_2 \le \pi$, it becomes a type of inverted pendulum and hence is unstable. To stabilize the system, the body support stiffness matrix (26) is compensated with joint torques exerted at the revolute joints. First, the null-space stabilization is considered. The joint torques in the null space $N(\mathbf{J}^T)$ must satisfy the equilibrium conditions. At the configuration in Fig. 5, the null-space joint torques meet the following conditions:

$$\begin{aligned}&\tau_{r1} = \tau_{\ell 1} = 0 \\ &\tau_{r2} = \tau_{\ell 2} = \tau_2 \\ &f_{r3} = f_{\ell 3} = f_3 \\ &2f_3\cos\theta_2 + 2\frac{\tau}{\ell}\sin\theta_2 + mg = 0\end{aligned} \tag{29}$$

where $\ell = \ell_{r3} = \ell_{\ell 3}$. With the joint torques of (29), the body support stiffness matrix is modified to

$$\begin{aligned}\mathbf{K}_p = \ & mg\bar{\mathbf{E}}_z + k_0(\bar{\mathbf{J}}_3^T\bar{\mathbf{J}}_3 + \bar{\mathbf{J}}_6^T\bar{\mathbf{J}}_6) - f_3\left(\bar{\mathbf{H}}_3 + \bar{\mathbf{H}}_6\right) \\ & - \tau_2\left(\bar{\mathbf{H}}_2 + \bar{\mathbf{H}}_5\right).\end{aligned} \tag{30}$$

Note that joint torque τ_2 can take both positive and negative values as long as it satisfies the last condition of (29). The positive joint torque, $\tau_2 > 0$, results in stabilizing the body support stiffness in certain directions, as will be demonstrated with numerical examples for a prototype SRL system in the following section. The null-space stabilization alone does not completely stabilize the system, but it reduces the active feedback control effort for stabilization.

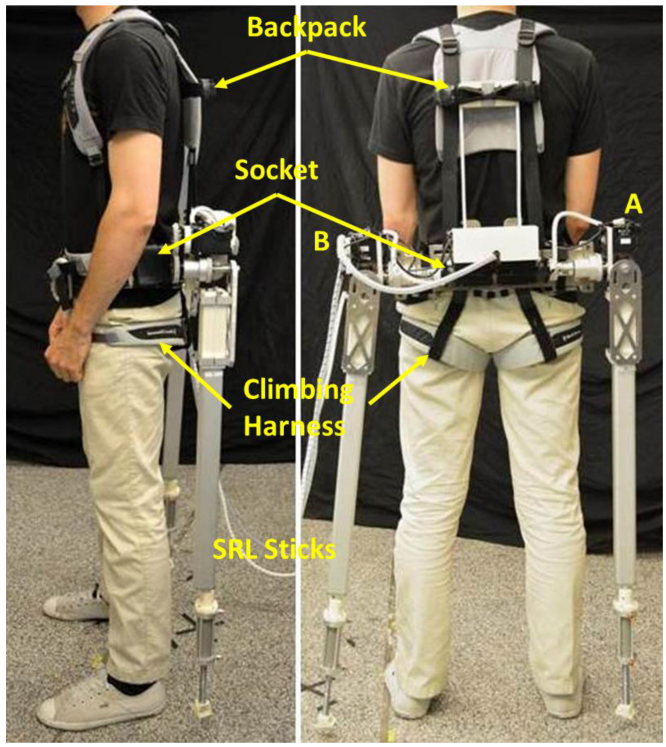

Fig. 6. Prototype of SRL system worn by a human around the waist.

IV. Implementation and Experiment

A. Prototype

A SRL prototype (see Fig. 6) has been developed in order to verify the load support strategy and control architecture that

have been derived and analyzed in the previous sections. The robot is worn with a backpack-like soft structure, equipped with shoulder straps and a climbing harness. The climbing harness has been modified to provide more support on the back side, allowing the user to lean on wide, soft straps when the robot is providing weight support. The bottom of the harness frame was shaped to fit the hip bone of a user by using 3-D printing technology. This 3-D-printed socket firmly secures the SRLs to the human, allowing for body support in all directions in the range space, and improves the comfort of the user. The prototype is equipped with two robotic limbs, having three DOFs each. The locations of the revolute joints were determined such that the center of the harness would be near the center of the total mass; that is, where Points C and H coincide. The light weight of the prototype and the proximity of its center of mass to the one of the human further increase user comfort.

Two rotational joints (actuated by Dynamixel Pro h54-100-s500-r servos, maximum continuous torque: 20 N·m) are placed at the base of the robotic limbs. Their axes intersect, forming an equivalent ball-and-socket joint. The third joint is prismatic (actuated by Firgelli FA-05-12-18 linear actuators, maximum force: 666 N, stroke: 0.46 m), and allows the robotic limbs to extend and retract in order to contact the environment and support the user. The prismatic joints are not backdrivable, due to a high gear ratio, so that they can bear the human with no actuator torque. The joint control loops run on microcontrollers in the robot base, while the high-level control commands, including reference configuration, actuator reference torques, and controller gains, are computed on a desktop PC and sent to the SRL.

The total weight of the robot is 13 kg. Power reaches the actuators through a power cord. The robot can become tetherless with a wireless link and a battery pack, resulting in an additional weight of 2 kg.

B. Numerical Computation

Using the parameter values and the specifications of the above prototype system, the body support stiffness is computed to verify the analytical results. Practical conditions, such as actuator torque limits, are taken into account in the following numerical examples.

First, we consider the symmetric configuration shown in Fig. 5. The eigenvalues of the body support stiffness matrix given by (26) are plotted in Fig. 7 against joint angle θ_2, $(\theta_{r2} = \theta_{\ell 2})$. In this plot, no stabilization control is considered. The sticks can bear the human load with no actuator torque because of the nonbackdrivable actuators. The sticks are treated as rods with a high structural stiffness $k_0 \gg 1$, which is equivalent to a high stiffness created by high gain joint servo in a quasi-static sense. We first consider the case in which the center of mass is located at the harness center, $h = 0$.

As shown in Fig. 7, one of the eigenvalues is zero for all configurations, indicating that the support stiffness matrix $K_{\rm p}$ is singular. When the joint angle is less than 90°, $0 \le \theta_2 < \pi/2$, all eigenvalues are positive except for the zero eigenvalue. The eigenvector associated with the zero eigenvalue reveals that the rotational motion of the human body about the y-axis is not constrained. A simple joint feedback control around the axes of $\theta_{r1}, \theta_{\ell 1}$ can produce positive servo stiffness, making the entire system stable.

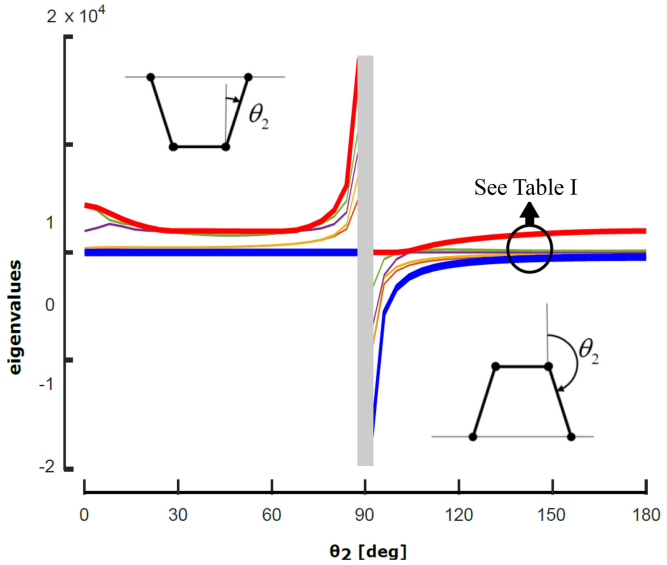

Fig. 7. Eigenvalues of support stiffness matrix $K_{\rm p}$ without stabilization control at the symmetric configuration [see (26)]. Red lines and blue lines indicate the maximal and minimal eigenvalues, respectively. At the gray zone of θ_2 near 90°, the SRL system cannot bear the human gravity load due to structural strength and actuator torque limits.

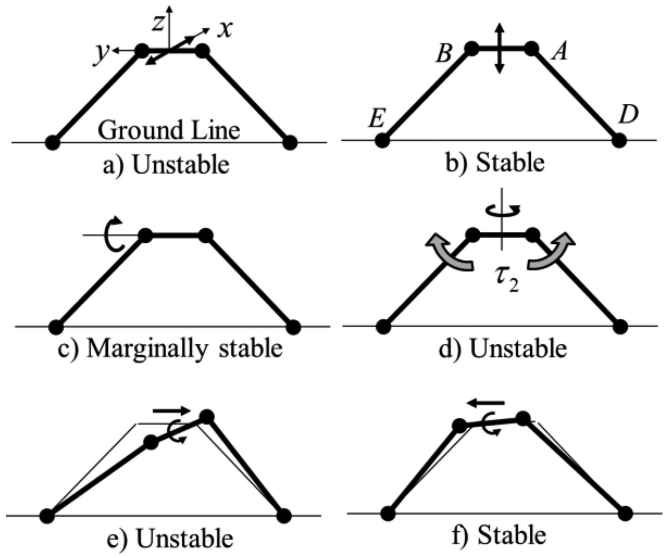

Fig. 8. Deformation mode shapes obtained from the eigenvectors of the support stiffness matrix $K_{\rm p}$ at the symmetric configuration with no stabilization control, $h = 0$. (a) Unstable. (b) Stable. (c) Marginally stable. (d) Unstable. (e) Unstable. (f) Stable.

In contrast, the system becomes unstable for $\pi/2 < \theta_2 \le \pi$, having some negative eigenvalues. Fig. 8 illustrates the six modes given by the eigenvectors associated with the individual eigenvalues, as listed in Table I. The mode in the x-axis translation is unstable; the SRL may fall in this direction [see Fig. 8(a)]. The mode in the z-axis translation is stable with a large eigenvalue due to the high structural stiffness of the sticks [see Fig. 8(b)]. The mode of rotation about the y-axis is marginally

TABLE I
EIGENVALUES AND EIGENVECTORS OF SUPPORT STIFFNESS MATRIX WITHOUT STABILIZATION CONTROL AT $\theta_2 = 145^\circ$

	mode	a	b	c	d	e	f
	eigenvalue	–980	133,550	0	–270	–380	77,580
eigenvector	x	1	0	0	0	0	0
	y	0	0	0	0	−0.3942	0.9190
	z	0	1	0	0	0	0
	phi1(roll)	0	0	0	0	0.9190	0.3942
	phi2(pitch)	0	0	1	0	0	0
	phi3(yaw)	0	0	0	1	0	0

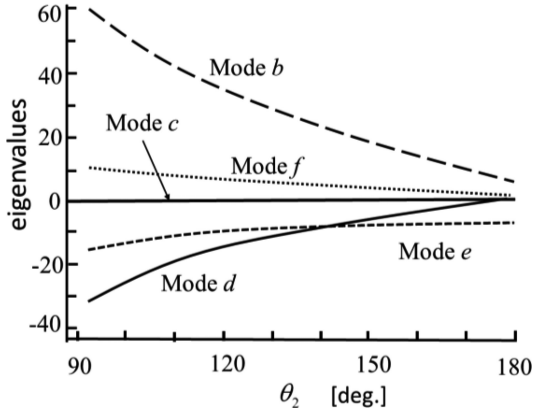

Fig. 9. Eigenvalues of support stiffness matrix $K_{\rm p}$ in the range space. The null-space stabilization moves the two unstable modes toward the stable range.

stable with zero eigenvalue [see Fig. 8(c)]. The z-axis rotation, on the other hand, is unstable; the SRL tends to collapse as it rotates about the z-axis [see Fig. 8(d)]. The SRL also tends to collapse sideways, as shown in Fig. 8(e). This mode is a combination of the y-axis translation and the x-axis rotation. In an orthogonal direction to the mode of Fig. 8(e), the stiffness matrix possesses a positive eigenvalue [see Fig. 8(f)]. In this direction, the sticks are compressed or extended, exerting a large restoring force with the spring constant k_0. These modes are called modes *a* through *f*.

Now consider the stabilization control to stabilize some of the unstable modes. Mode *a* in Fig. 8 cannot be stabilized, since it is outside the range space; the SRL system is free to rotate about the ground line. The remaining five modes are within the range space and can be stabilized. For mode *c*, joint feedback control around the axes of $\theta_{r1}, \theta_{\ell 1}$ is required for generating positive servo stiffness, as in the case of $0 \leq \theta_2 < \pi/2$. Two other unstable modes *d* and *e* must be stabilized. It is interesting to note that null-space stabilization can contribute to the stabilization of modes *d* and *e*.

Fig. 9 shows the eigenvalues of the support stiffness matrix with null-space stabilization based on (30). Both unstable modes *d* and *e* get closer to the stable region with the null-space stabilization. Comparison of the eigenvalues between Fig. 7 (without null-space stabilization) and Fig. 9 (with null-space stabilization) indicates that the two unstable eigenvalues in Fig. 7, i.e., –270 and –380, are shifted to approximately –10 in Fig. 9 around $\theta_2 = 145^\circ$. Positive torques applied to both θ_{r2} and $\theta_{\ell 2}$ joints increase the internal tension that tends to expand the closed-loop linkage comprising the two sticks, the harness socket, and the ground line [see Fig. 8(d)]. These joint torques, although kept constant, generate resistive effects against collapsing movements illustrated in Fig. 8(d) and (e).

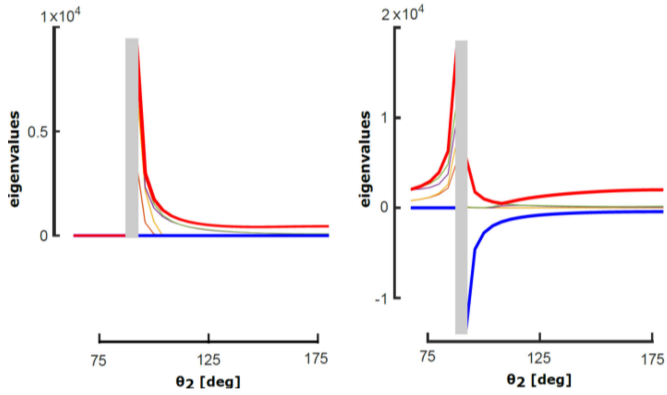

Fig. 10. Eigenvalues of support stiffness matrix with full stabilization control. (a) Contributions of the joint servo stiffness alone. (b) Total stiffness with both null-space stabilization and joint servo stiffness control.

Null-space stabilization alone cannot stabilize the system in the entire range space. We need to add joint servo stiffness with the feedback gain given by (22). Fig. 10(a) shows the eigenvalues of the support stiffness matrix due to the joint servo stiffness, $\bar{\mathbf{J}}^T \mathbf{K}_q \bar{\mathbf{J}}$, and Fig. 10(b) shows the overall stiffness including both null-space stabilization and the joint servo stiffness control. All the modes were made stable except mode *a*, which cannot be stabilized. The eigenvalues of the six modes at $\theta_2 = 145^\circ$ are –546, 1695.4, 110.3, 1.4, 4.1, and 172.5, respectively.

The effectiveness of the null-space stabilization varies depending on the configuration, θ_2. If it requires a large toque, it may exceed the torque limit: $0 < \tau_2 \leq \tau_{2\,\max}$. To quantify the effectiveness of the null-space stabilization, the difference between the matrix norm of the gain matrix without the null-space stabilization and that with the null-space stabilization is evaluated for the following diverse configurations:

$$C = |K_{q-\text{no null space}}| - |K_{q-\text{with null space}}|\,. \qquad (31)$$

If this value *C* is positive, the null-space stabilization is effective. Fig. 11 shows the value *C* against joint angle θ_2. Note that the null-space stabilization works effectively for larger θ_2.

The height of the total mass, h, plays an important role in stability. In particular, the system can be stabilized if the harness center can be raised higher than the total mass center, i.e., a negative h in Fig. 5. As given by (24), raising the harness center yields a positive stiffness to the fourth and fifth diagonal components of the Hessian $\bar{\mathbf{E}}_z$. These contribute to stabilizing modes *c* and *e* in Fig. 8. This arrangement of SRLs is similar to "clutches" that hold the body under the arms. It is, however, cumbersome to raise the harness too high since it may interfere with the human's upper body motion. It is a design trade-off between stability and ease of work.

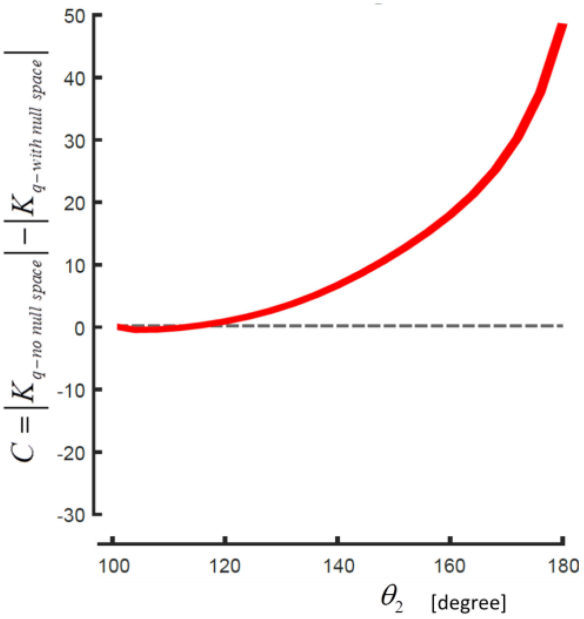

Fig. 11. Effectiveness of combined null-space stabilization and joint servo stiffness compared with joint servo alone. The gain matrix norm for the combined control is smaller.

So far, we have examined a simple symmetric configuration case (see Fig. 5) to illustrate the effects of the proposed stabilization techniques. However, depending on the environment, such a symmetric configuration may not be allowed, or a nonsymmetric configuration may provide a better result. The analytical formulation of the problem presented in this study is completely general and can be applied to any 3-D configuration of the robot. As an example of 3-D analysis, we now consider all the possible SRL configurations left that correspond to a given right SRL position. The length of both SRLs is fixed at $\ell_{r3} = \ell_{\ell 3} = \ell_{\max}$. Fig. 12 plots the eigenvalues of K_{p} for every configuration in the workspace of the left SRL. The blue bar represents the (fixed) configuration of the right SRL. Fig. 12(a) shows the minimum eigenvalue of K_{p} when no stabilization control is used. To meet the equilibrium condition, it is assumed that the human exerts a necessary force $\mathbf{F}_h$. The system is unstable or marginally stable for the entire configurations of the left SRL. The stabilization control makes the system stable in the range space. Fig. 12(b) plots the minimum eigenvalue in the range space, which is positive for all the left SRL configurations. This plot not only shows that the system is stable but also indicates the level of stability, i.e., the stiffness in the worst direction. Note that a large minimum eigenvalue is obtained for the left SRL configuration shown by the yellow bar in Fig. 12(b). Fig. 12(c) compares the feedback control effort with and without null-space stabilization. The use of null-space stabilization is beneficial when the difference in norms assumes a large positive value. It can be noticed that null-space stabilization should be used in many SRL configurations, especially when the two SRL sticks are pointing in opposite directions. In these cases, the robot is able to exert much higher internal forces without producing effects on the overall balance of the system.

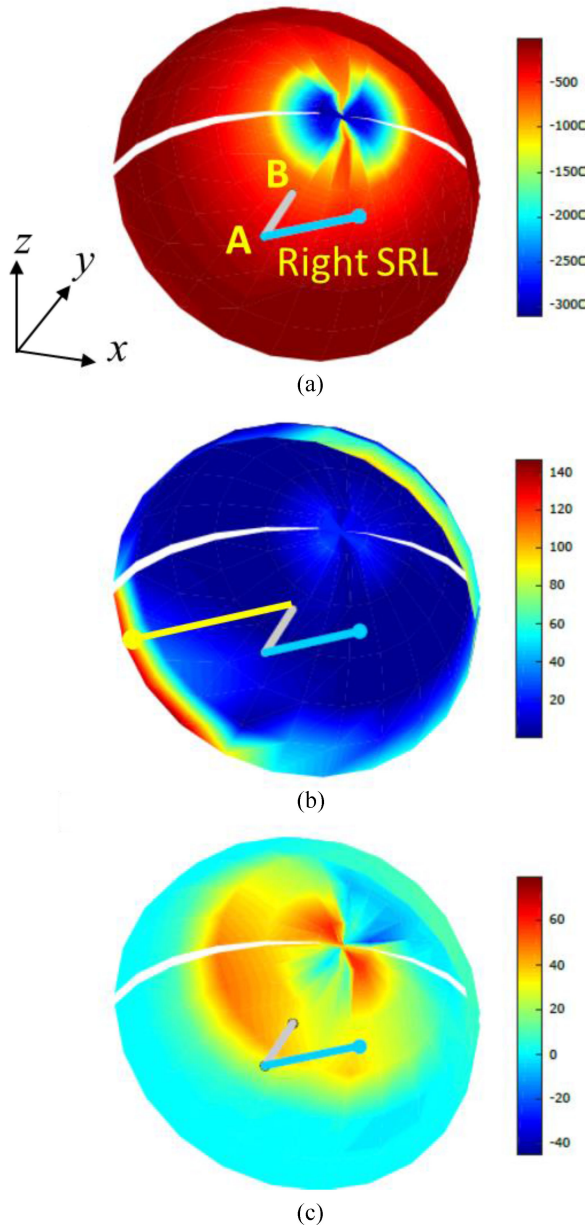

Fig. 12. Computations for 3-D SRL configurations. The right robotic limb (blue bar) is placed at $\theta_{r1} = 56°, \theta_{r2} = 34°$, and the left robotic limb is placed at various locations within its workspace (which has the shape of a hemisphere, since the length of the robotic limb is fixed). The base of the robot is represented by a grey bar. Plot (a) shows the minimum eigenvalue of K_{p} when no stabilization control is used. This value is not positive in the workspace; therefore, the system is unstable or marginally stable. Plot (b) shows the minimum eigenvalue in the range space, when the stabilizing controller (null space and P control) is applied. The system has been stabilized everywhere, and the stabilization is most effective when the robot is in a symmetric configuration (left robotic limb represented by yellow bar). Plot (c) shows the utility of null-space stabilization, which is advantageous when the plotted c values [see (31)] are positive.

C. Experimental Evaluation

The stabilization of the SRL system has been tested at the symmetric planar configuration shown in Fig. 5 ($\theta_2 = 145°$). The experimental setup is shown in Fig. 13(a). The end effectors of the robot are secured to the ground with 3-D printed ball-and-socket joints, which are free to rotate.

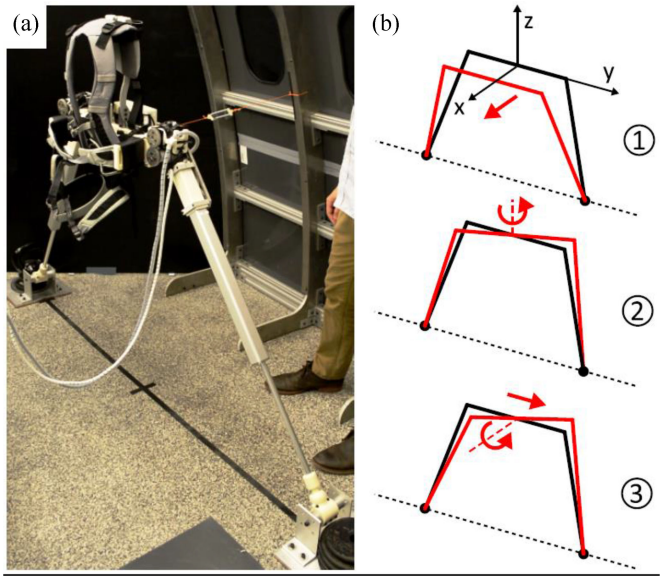

Fig. 13. Experimental setup for stiffness tests.

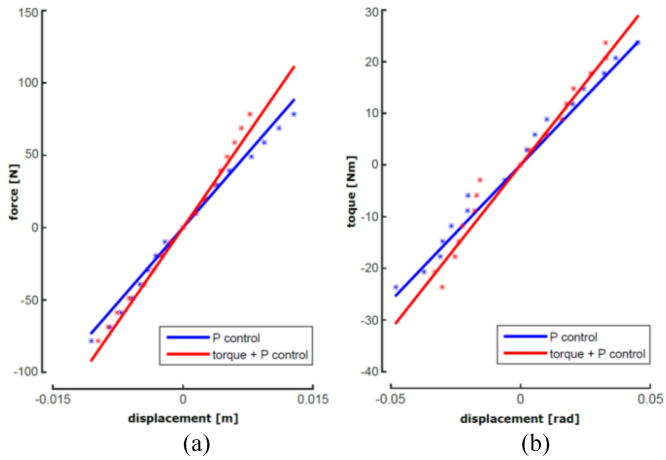

Fig. 14. Experimental results of stiffness tests. Straight lines are theoretical prediction, while dots are experiment. Blue is joint stiffness control only, and red is combined stabilization.

These simplified joints are used because the goal of the experiment is to study the stability of the robot, assuming that it is secured to the environment. In a realistic scenario, the contact of the robot to the environment must be ensured by end effectors that are lightweight, produce a strong holding force, and are easily detachable. Examples of suitable end effectors include electromagnets and vacuum grippers [18]. In order to orient these systems parallel to the environment, it is possible to add one or more wrist DOFs to the robot's wrists. A simpler and lighter solution is represented by compliant passive wrists that can adapt to the shape of the environment when the robotic limbs push against it. Accurate positioning of the robotic grippers is not needed for the control algorithm to work. Once the end effectors are secured to the ground, it suffices to read the joint positions from the onboard sensors in order to optimize the controller and stabilize the human as described in this study.

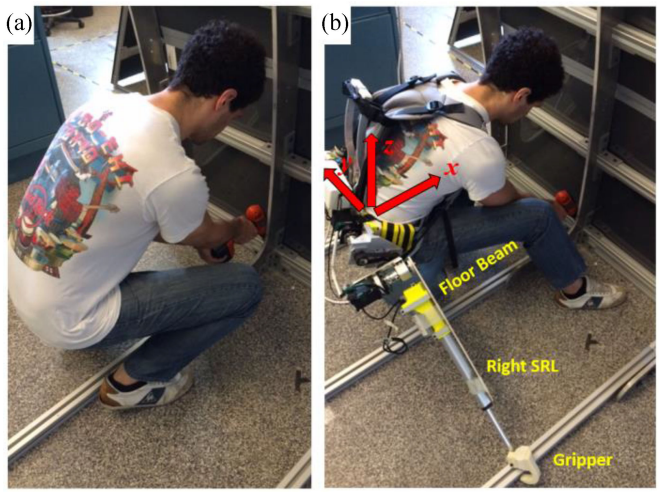

Fig. 15. Typical application of body support with the SRL system.

Without stabilization control, the body support stiffness matrix K_{p} has three unstable (negative) eigenvalues, as shown in Fig. 13(B). The x-axis translation [see ① in Fig. 13(b)] is unstable and cannot be stabilized. A cable with a soft serial spring was used for preventing the SRL system from falling in the x-axis direction during experiments. The objective of experiments is to stabilize modes d and e [see ② and ③ in Fig. 13(b)]. Restoring force and moment making these modes stable were measured to evaluate the stiffness in each mode.

Two control strategies were tested. First, the SRL system was stabilized using only joint servo stiffness control. Second, the null-space stabilization control was added to the joint stiffness control using the same joint feedback gains as the first case. Fig. 14 shows the results. Fig. 14(a) plots the restoring force against the y-axis displacement (mode e). The straight lines represent the theoretical prediction based on the model of the support stiffness matrix. The stiffness without null-space stabilization was 6.88×10^3 N/m, whereas the stiffness with the null-space stabilization using constant joint torques, $\tau_{r2} = \tau_{\ell 2} = 10$ N·m, achieved 8.66×10^3 N/m of stiffness.

Fig. 14(b) shows the restoring moment against rotational displacement about the z-axis. Without the null-space stabilization, the rotational spring constant was 5.26×10^2 N·m/rad, while the one with the null-space stabilization was 6.36×10^2 N·m/rad. The use of constant null-space torques has a stabilizing effect on the SRL base. This can be observed both for the linear stiffness in the y-direction (which increases by 25% with the addition of null-space torques) and for the rotational stiffness around the z-axis (which increases by 21% with the addition of null-space torques).

The stabilization control can be incorporated into the entire SRL control system for assisting a human in practical scenarios. Fig. 15 illustrates a typical application of the SRL system to aircraft assembly. The worker bends to reach a lower section of the fuselage, taking a fatiguing posture for a long time [see Fig. 15(a)]. Similar tasks can be found in many applications where workers have to work on large structures, such as a ship, a building, or plant equipment. Crouching and standing repeatedly

are laborious. The SRL with two high-force prismatic joints can lift or lower the human body, while securing its grippers to the floor beams. The human body can be supported stably with the stabilization control. Although the movement in the x-direction is unstable, the human not only supports the body, but also adjusts the distance to the wall with his legs on the floor [see Fig. 15(b)]. All the other directions can be supported stably with an appropriate compliance. Often the human has to change posture slightly, e.g., moving sideways (mode e) or rotating about the z-axis (mode d). The stiffness of modes d and e can be tuned to provide the human with sufficient stability as well as with freedom to change the posture. The stiffness demonstrated in the above experiment was found to be adequate to meet these requirements. Unlike a passive stool, the SRL is capable of supporting the human with tunable stiffness as well as of lifting and lowering the human in crouching and standing.

V. Conclusion

A new type of SRL with high-force prismatic joints has been developed for supporting the wearer's body in taking fatiguing postures or working in a dangerous environment. The stiffness matrix with which the body is supported has been analyzed. Two control methods for stabilizing the body support have been presented: the null-space stabilization using Hessian matrices and joint servo stiffness control based on the Jacobian. The two extra-limb structure is kinematically singular, creating a null space where a particular combination of joint torques does not disturb the balance of forces, yet influences the stiffness and quasi-static stability of the system. The joint torques in the null space can contribute to stabilizing the system without active feedback control. The control methods have been implemented on a prototype SRL system. Unlike a standard stool or a passive body support gear, the SRL system can support a human with tunable body support stiffness; therefore, the human can change the posture freely and stably. With the active joints, the SRL can also lift or lower the body for assisting the human in crouching and standing repeatedly.

References

[1] Bureau of Labor Statistics, "Census of Fatal Occupational Injuries Summary," 2013.

[2] Occupational Safety and Health Administration (OSHA) Standards For Construction Industry, *Duty to Have Fall Protection*, Standard 1926.501.

[3] T. Brown, "Injuries, illnesses and fatalities in manufacturing, 2005," U.S. Bureau of Labor Statistics, 2007.

[4] A. Mosisa and S. Hipple, "Trends in labor force participation in the United States," *Monthly Labor Rev.*, vol. 129, no. 10, pp. 35–57, 2006.

[5] A. Dollar and H. Herr, "Lower extremity exoskeletons and active orthoses: Challenges and state-of-the-art," *IEEE Trans. Robot.*, vol. 24, no. 1, pp. 144–158, Feb. 2008.

[6] H. Kazerooni, J.-L. Racine, L. Huang, and R. Steger, "On the control of the Berkeley lower extremity exoskeleton (BLEEX)," in *Proc. IEEE Int. Conf. Robot. Autom.*, 2005, pp. 4353–4360.

[7] H. Kawamoto and Y. Sankai, "Power Assist System HAL-3 for Gait Disorder Person," in *Computers Helping People with Special Needs*, vol. 2398, K. Miesenberger, J. Klaus and W. Zagler, Eds. Berlin, Germany: Springer, 2002, pp. 196–203.

[8] Lockheed Martin Corp., (2014, Nov.). "Relief for the Daily Grind: Industrial Exoskeletons at Work," Press Release, [Online]. Available: http://www.lockheedmartin.com/us/news/features/2014/mfc-103114-relief-daily-grind-industrial-exoskeletons-work.html

[9] T. Nef, M. Guidali, and R. Riener, "ARMin III—Arm therapy exoskeleton with an ergonomic shoulder actuation," *Appl. Bionics Biomech.*, vol. 6, no. 2, pp. 127–142, 2009.

[10] J. W. Raade and H. Kazerooni, "Analysis and design of a novel hydraulic power source for mobile robots," *IEEE Trans. Autom. Sci. Eng.*, vol. 2, no. 3, pp. 226–232, Jul. 2005.

[11] C. J. Walsh, K. Endo, and H. Herr, "A quasi-passive leg exoskeleton for load-carrying augmentation," *Int. J. Humanoid Robot.*, vol. 4, no. 3, pp. 487–506, 2007.

[12] P. D. Neuhaus, J. H. Noorden, T. J. Craig, T. Torres, J. Kirschbaum, and J. E. Pratt, "Design and evaluation of mina: A robotic orthosis for paraplegics," in *Proc. IEEE Int. Conf. Rehabil. Robot.*, 2011, pp. 1–8.

[13] M. Wehner, B. Quinlivan, P. M. Aubin, E. Martinez-Villalpando, M. Baumann, L. Stirling, K. Holt, R. Wood, and C. Walsh, "A lightweight soft exosuit for gait assistance," in *Proc. IEEE Int. Conf. Robot. Autom.*, 2013, pp. 3362–3369.

[14] M. Abdoli-Eramaki, J. Stevenson, S. Reid, and T. Bryant, "Mathematical and empirical proof of principle for an on-body personal lift augmentation device (PLAD)," *J. Biomech.*, vol. 40, no. 8, pp. 1694–1700, 2007.

[15] M. Wehner, D. Rempel, and H. Kazerooni, "Lower extremity exoskeleton reduces back forces in lifting," in *Proc. ASME Dynamic Syst., Control Conf.*, 2009, pp. 49–56.

[16] F. Parietti and H. Asada, "Dynamic analysis and state estimation for wearable robotic limbs subject to human-induced disturbances," in *Proc. IEEE Int. Conf. Robot. Autom.*, 2013, pp. 3880–3887.

[17] F. Parietti and H. Asada, "Supernumerary robotic limbs for aircraft fuselage assembly: Body stabilization and guidance by bracing," in *Proc. IEEE Int. Conf. Robot. Autom.*, 2014, pp. 1176–1183.

[18] F. Parietti, K. Chan, and H. Asada, "Bracing the human body with supernumerary robotic limbs for physical assistance and load reduction," in *Proc. IEEE Int. Conf. Robot. Autom.*, 2014, pp. 141–148.

[19] H. Asada and J.-J. Slotine, *Robot Analysis and Control*. New York, NY, USA: Wiley, 1986.

Federico Parietti (S'11) received the B.S. degree in mechanical engineering from Politecnico di Milano, Milan, Italy, and the double M.S. degree from Politecnico di Milano and Politecnico di Torino, Turin, Italy, in 2008 and 2011, respectively. He is currently working toward the Ph.D. degree in mechanical engineering with d'Arbeloff Laboratory for Information System and Technology, Mechanical Engineering Department, Massachusetts Institute of Technology, Cambridge, MA, USA.

In 2010, he was a Visiting Student with the Department of Mechanical Engineering, ETH Zurich, Zurich, Switzerland. In 2011, he was a Visiting Scholar with the Robotics Institute, Carnegie Mellon University, Pittsburgh, PA, USA. His research interests include wearable robotics, man–machine interfaces, and human augmentation.

Harry Asada (M'89) received the B.S., M.S., and Ph.D. degrees in precision engineering in 1973, 1975, and 1979, respectively, all from Kyoto University, Kyoto, Japan. He specializes in robotics, biological engineering, and system dynamics and control.

He is currently the Ford Professor of Mechanical Engineering and Director of the Brit and Alex d'Arbeloff Laboratory for Information Systems and Technology, Department of Mechanical Engineering, Massachusetts Institute of Technology (MIT), Cambridge, MA, USA. His current robotics research includes wearable robots, cellular PZT actuators, and robot applications to aircraft manufacturing and nuclear power plant monitoring. His research in the bio area focuses on biointegrated robots, in which live cells and tissues are used as components.

Dr. Asada received Best Paper Awards at the IEEE International Conference on Robotics and Automation in 1993, 1997, 1999, and 2010; the O. Hugo Schuck Best Paper Award from the American Control Council in 1985; Best Journal Paper Awards from the Society of Instrument and Control Engineers in 1979, 1984, and 1990; and the Best Journal Paper Award from the Journal of Advanced Robotics in 2002. He received the Henry Paynter Outstanding Researcher Award from the American Society of Mechanical Engineers (ASME) the Dynamic Systems and Control in 1998. More recently, he received the 2011 Rufus Oldenburger Medal from ASME, and Ruth and Joel Spira Award for Distinguished Teaching from the School of Engineering, MIT. He is a Fellow of ASME.